Journal of Materials Chemistry A

Accepted Manuscript

ROYAL SOCIETY OF CHEMISTRY

www.rsc.org/materialsA

Journal Name

RSCPublishing

ARTICLE

Fabrication of urchin-like Ni-$Co_2(CO_3)_{1.5}(OH)_3$@$NiCo_2S_4$ on the Ni foam by ion exchange route and applying to asymmetric supercapacitor

Cite this: DOI: 10.1039/x0xx00000x

Received 00th January 2012,
Accepted 00th January 2012

DOI: 10.1039/x0xx00000x

www.rsc.org/

Bin Yang,[a] Lei Yu,[a] Huijun Yan,[a] Yanbo Sun,*[b] Qi Liu,[a] Jingyuan Liu,[a] Dalei Song,[a] Songxia Hu,[c] Yi Yuan,[a] Lianhe Liu,[b] Jun Wang*[ac]

The transition metal oxides/sulfides which are pesudocapacitor electrode materials have been extensively investigated and demonstrated a fast energy storage process, but the low rate performance and worse cycle stability are serious problems for the practical application. Hence, we presented a concept which is designing the architecture of electrode materials to further improve the characteristic of pesudocapacitor electrode materials which are rate performance and cycle stability by the interface ion exchange. The complete fabrication process is that the precursors which were obtained by hydrothermal reaction soaked into the NaHS aqueous solution to synthesize the urchin-like core-shell structure of Ni-$Co_2(CO_3)_{1.5}(OH)_3$@$NiCo_2S_4$. The core-shell nanostructure electrode materials can make full use of both components and exhibits a potential synergistic effect. At the same time, the electrochemical measurement witnessed an excellent result, which is 956.4 F g^{-1} at current density of 4 A g^{-1} under three-electrode system measurement and the actual energy density of 32.3 W h kg^{-1} and power density of 1835W kg^{-1} for the asymmetric supercapacitor.

1. Introduction

As for the pseudocapacitance electrode materials, the transition metal oxides/sulfides that the capacitive electrochemical features is the redox pseudocapacitance have been extensively attention, because the power density of the pseudocapacitor is higher than battery and the energy density is higher than double electron layer capacitance.[1-6] This is attributed to high-efficiency and reversible electrochemical reaction on the electrode surface to storage the charge.[7-10] Nevertheless, the transition metal oxides/sulfides are semiconductor and a wide band gap compounds, leading to a larger internal resistance and low rate performance.[11-14] Actually, the above-mentioned problems are the low rate of ion absorption-desorption and electron transfer from the interface of electrode-electrolyte to the current collector.

Therefore, it is urgent to transform the low rate of ion and electron transfer by the electrode material architecture design.[15-20] At the same time, more researchers obtained the satisfactory results with several architecture design means, including the situ growth on the conductive substrates, synthesis of the advanced nanostructure materials and compositing with the carbon materials.[21-25] According to the electron and ion transfer process, the architecture design is mainly to be divided into three parts (as shown in Fig. 1): (1) electrode-electrolyte interface (2) crystal structure electrode materials (3) the connection between electrode materials and current

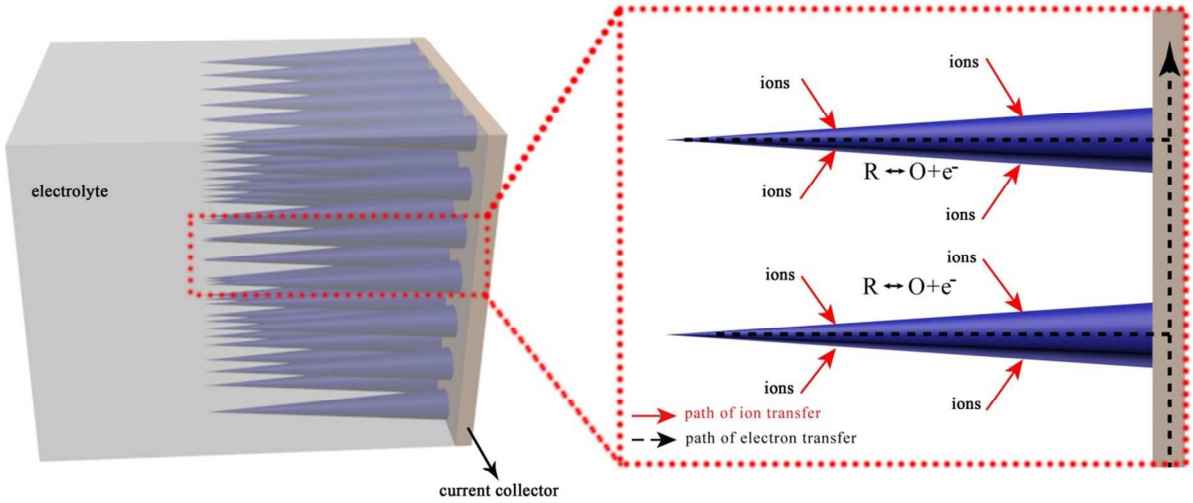

Fig. 1 the image of the ion and electron transfer path in the electrochemical process.

collector. The electrode-electrolyte interface design is that synthesis of advanced nanostructure materials which has high specific area, suitable mesoporous and high electrochemical response accelerate the ion transport rate and sufficiently use the electroactive materials. The crystal structure design of electrode materials is improving the electron transfer rate and reducing electron transfer resistance in the internal electrode materials to decrease the energy loss. Due to the metal oxides/sulfides electrode has a poor conductivity, doping the other element is an efficient path to intensify degree of the crystal defect and enhance the conductivity capability.[26,27] The bimetal electroactive materials, which are one metal ion replacing the other metal ion, have been demonstrated a high ion and electron transfer rate because the electroactive materials have complex chemical compositions and don't change the crystal structure.[4,28-31] The connection between electrode materials and current collector design is that selecting a fit conductivity substrate directly connects with electroactive materials without binder to increase the rate of electron transport and reduce the percentage of inactive materials.

Recently, the transition metal sulfides have attracted wide interest for the energy storage, because of the fast ion transfer rate and high electrochemical response, especially the bimetal sulfides.[32-35] The nanostructure $NiCo_2S_4$ has been demonstrated an excellent application prospect for electrocatalysis, solar cells and energy storage.[4,36,37] Therefore, we can design the electrode materials architecture by the interface of ion exchange which are a part of urchin-like precursors ($NiCo_2(CO_3)_{1.5}(OH)_3$) replaced to the $NiCo_2S_4$ on the precursors to form the urchin-like core-shell structure on the Ni Foam (conductivity substrates). It thorough gives expression to the characteristic of the electrode material architecture design as follows: (1) The electroactive materials which directly grow on the conductivity substrate have been demonstrated a higher utilization rate than tradition electrode materials which is electroactive and binder materials coating on the conductivity substrate. (2) The shell structure ($NiCo_2S_4$) exhibits a high electrochemical response capability and the core structure ($NiCo_2(CO_3)_{1.5}(OH)_3$) shows an excellent cycle stability, indicating that the core-shell electrode materials present a high rate performance and excellent cycling stability. (3) The Ni Foam as the conductivity substrates can provide more sites to load more electroactive materials (electroactive mass of urchin-like core-shell structure: 6.4 mg. cm^{-3}) and has a high rate of electron transfer on the conductivity substrate. Hence, the measurement of electrochemical performance exhibits a satisfactory result. In the three-electrode system of electrochemical measurement, it shows specific capacitance of 956.4 F g^{-1} at the current density of 4 A g^{-1} and the specific capacitance still remains 80.1% overall the capacitance after 5000 cycles. In the two-electrode system, the urchin-like $NiCo_2(CO_3)_{1.5}(OH)_3$ @$NiCo_2S_4$ as a positive electrode and activated carbon (AC) as a negative electrode demonstrate a higher actual energy density of 32.3 W h kg^{-1} and power density of 1835 W kg^{-1} at current

density of 4 A g^{-1}. At the same time, the measurement result of cycle stability is that the specific capacitance remains 84.1% of initial capacitance after 5000 cycles.

2. Experiment

2.1 Fabrication of the urchin-like precursors:

All the chemicals are of analytical grade and were used without further purification except NaHS (purify: 68~72%, chemical formula: $NaHS.xH_2O$, Aladdin Industrlal Corporation). The Ni Foam was pretreated with 3M HCl, acetone or ethanol by ultrasonic washing 20 min, respectively. The 20mmol $Co(NO_3)_2.6H_2O$ and 10mmol $Ni(NO_3)_2.6H_2O$ were dissolved in 100mL deionized water. The Co and Ni salts mixture solution dropwise added into 100mL of 15mmol Triton X-100 (Nonionic surfactant, chemical formula: $C_{34}H_{62}O_{11}$, Tianjin Guangfu Fine Chemical Research Institute) aqueous solution and stirred 30min. Then, 60mmol urea added in the solution and stirred 3h. At last, the mixture solution transferred into a 50 mL Teflon-lined stainless steel autoclave and the cleaned Ni foam was immersed into reaction solution maintaining at 120 ^oC for 24 h. After reaction, the Ni foam was washed with deionized water to remove surfaces ion and vacuum dried in 60 ^oC for 24h. After the ICP test for the different concentrations of the samples solution, the average atomic ratio of Co and Ni element is 2.02:1. Therefore, the chemical formula of precursor is $NiCo_2(CO_3)_{1.5}(OH)_3$.

2.2 Fabrication of the urchin-like $NiCo_2S_4$ and $Ni-Co_2(CO_3)_{1.5}(OH)_3@NiCo_2S_4$:

Fabrication process of the urchin-like $NiCo_2S_4$ is the precursors on the Ni Foam reacted with the 5mmol L^{-1} Na_2S aqueous solution in a 50 mL Teflon-lined stainless steel autoclave at 160 ^oC for 6h. Fabrication process of the urchin-like $NiCo_2(CO_3)_{1.5}(OH)_3@NiCo_2S_4$ is precursors on the Ni Foam were immersed into 5mmol L^{-1} NaHS aqueous solution for 2 days.

After reaction, the Ni Foam was washed and vacuum dried in 60 ^oC for 24h.

2.3 Fabrication of the $NiCo_2(CO_3)_{1.5}(OH)_3@NiCo_2S_4$ nanowires:

The fabrication process of the precursors nanowires were the same with the urchin-like precursors, except that the reaction time is 12h. The precursor nanowires were immersed into 5mmol L^{-1} NaHS aqueous solution for 2 days and then washed, dried.

2.4 Fabrication of the Activated carbon (AC) electrode:

First, the commercial AC, acetylene black and polyvinylidenedifluoride (PVDF) at ratio of 85:10:5 were uniformly dispersed in alcohol. And then the homogeneous paste was pressed onto Ni Foam (1×1 cm^2). Finally, the fabricated electrode was dried under vacuum at 60 ^oC for 1 day.

2.5 Measurement the weight of active materials:

The mass of cleaned Ni foam is 14.3 mg cm^{-2} by the electronic balance weighting. After the sulfuration process with NaHS aqueous solution, the total mass of Ni foam with $Ni-Co_2(CO_3)_{1.5}(OH)_3@NiCo_2S_4$ is 20.7 mg cm^{-2} by the electronic balance weighting. Therefore, the mass of urchin-like $Ni-Co_2(CO_3)_{1.5}(OH)_3@NiCo_2S_4$ is 6.4 mg cm^{-2}.

2.6 Characterization:

The morphologies of the products were observed by scanning electron microscope (SEM; JEOL JSM-6480A microscope, Tokyo, Japan) and transmission electron microscope (TEM; FEI company Tecnai G2 20 S-twin, 200kV). The crystalline structure was characterized by X-ray-diffraction system (XRD, Rigaku TTR-III) equipped with Cu Kα radiation (λ=0.15406nm). The X-ray photoelectron spectroscopy (XPS, ESCALAB 250Xi) and Energy-dispersive spectroscopy (EDS, JEOL JSM-6480A microscope, Tokyo, Japan) were employed to investigate the elemental compositions of the samples. The chemical formula of precursors is determined by inductively coupled plasma spectrometer (Bruker 820-MS ICP-MS instrument).

2.7 Electrochemical measurement:

The electrochemical measurement of all the samples was investigated under a three-electrode cell configuration with 2 M KOH electrolyte at 25 ^oC. The Ni Foam supporting the urchin-like and nanowires were acted as a work electrode. The saturated calomel electrode and Pt foil were acted as reference electrode and counter electrode, respectively.

The asymmetric supercapacitor is assembled by the urchin-like $NiCo_2(CO_3)_{1.5}(OH)_3@NiCo_2S_4$ on the Ni foam as positive electrode and AC as negative electrode with 6M KOH electro lyte. The quality ratio of positive and negative electrodes was

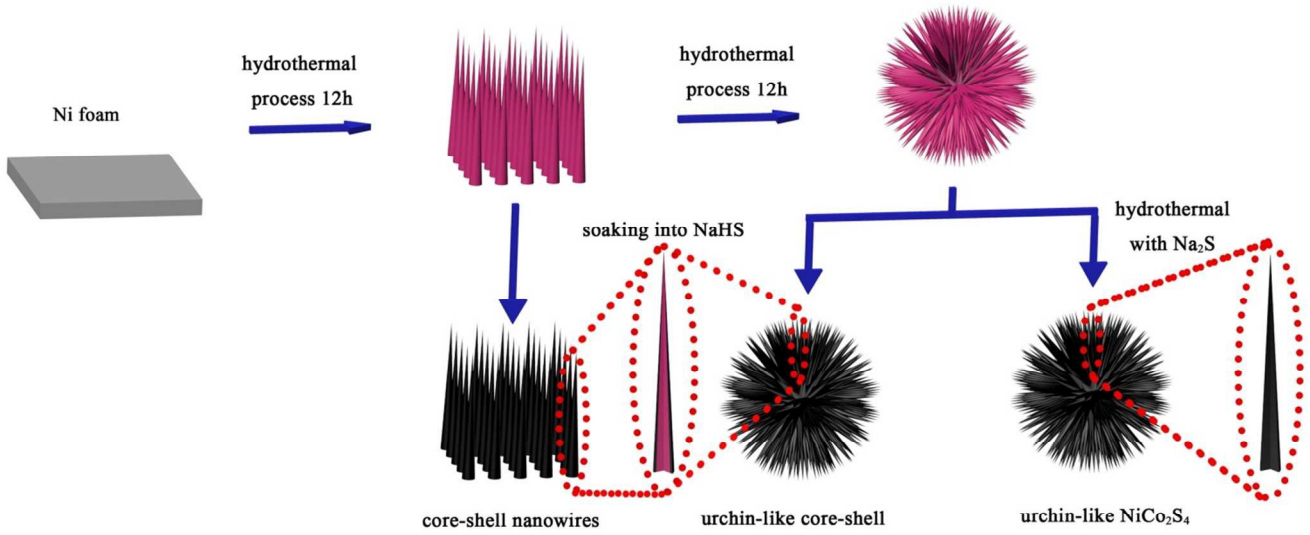

Fig. 2 schematic illustration of synthetic urthin-like $NiCo_2S_4$ and $NiCo_2(CO_3)_{1.5}(OH)_3$@$NiCo_2S_4$ and $NiCo_2(CO_3)_{1.5}(OH)_3$@$NiCo_2S_4$ nanowires on the Ni Foam.

calculated by equation (1) as follows:

$$\frac{m_+}{m_-}=\frac{C_-\times\Delta E_-}{C_+\times\Delta E_+} \quad (1)$$

Where C (F g-1) is the specific capacitance of positive and negative electrodes, ΔE is the potential change during the discharge at the three-electrode cell measurement. The specific capacitance of each electrode was calculated from the charge-discharge curves for the following equation (2):

$$C=\frac{I\times t}{m\times\Delta E} \quad (2)$$

Where I (A) is a current density at discharge process, t (s) is a discharge time, m (g) is a mass of electroactive materials. All of the above measures were conducted on a CHI 760B electrochemical workstation (ShangHai CH Instrument Company, China).

3. Result and discussion

3.1 Reaction mechanism:

The fabrication processes of highly ordered urchin-like precursor, $NiCo_2S_4$ and $NiCo_2(CO_3)_{1.5}(OH)_3$@$NiCo_2S_4$ and $NiCo_2(CO_3)_{1.5}(OH)_3$@$NiCo_2S_4$ nanowires on the Ni foam are schematically illustrated in Fig. 2. The precursor nanowires were fabricated via a hydrothermal process which is Co and Ni nitrate reacted with urea under the Triton X-100 as surfactant condition after 12h. When the reaction time increased to 24h, a large number of precursor nanowires aggregated into the urchin-like structure on the Ni foam. The nanowires precursor on the Ni Foam was immersed into 5mmol L^{-1} NaHS aqueous solution to fabricate the $NiCo_2(CO_3)_{1.5}(OH)_3$@$NiCo_2S_4$ nanowires. The urchin-like $NiCo_2(CO_3)_{1.5}(OH)_3$@$NiCo_2S_4$ were fabricated by the same means. The fabrication process of urchin-like $NiCo_2S_4$ was hydrothermal process with Na_2S. Fig. S1 exhibits the photography of urchin-like precursors (left), $NiCo_2S_4$ (middle) and $NiCo_2(CO_3)_{1.5}(OH)_3$@$NiCo_2S_4$ (right).

3.2 Materials Characterization:

The SEM image exhibits $NiCo_2(CO_3)_{1.5}(OH)_3$@$NiCo_2S_4$ nanowires uniformly grow on the Ni Foam, as shown in Fig. 3a. Fig. 3b shows that a large number of nanowires aggregated and formed the urchin-like structure in the low magnification SEM image with the time of hydrothermal reaction increasing to 24h. This attributed to the surfactant assisting the nanowires aggregation. Fig. 2Sa shows SEM image of precursor nanowires. Fig. 2Sb and c shows the urchin-like precursors and $NiCo_2S_4$. Compared with the morphology of precursor nanowires or urchin-like precursors, the morphology of $NiCo_2(CO_3)_{1.5}(OH)_3$@$NiCo_2S_4$ and $NiCo_2S_4$ did not change. As for the transition metal sulfides electrode materials which has

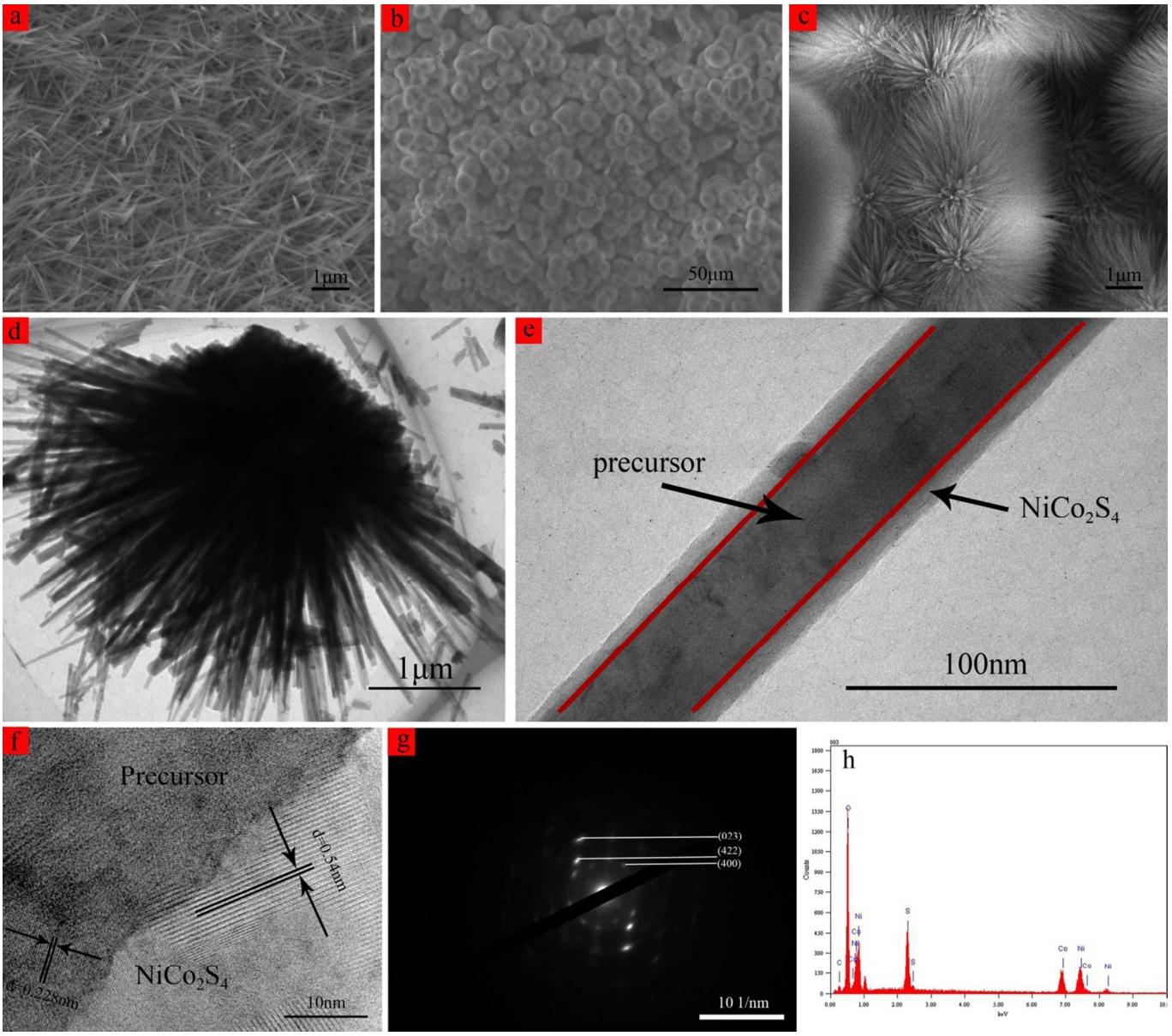

Fig. 3 (a) SEM image of $NiCo_2(CO_3)_{1.5}(OH)_3$@$NiCo_2S_4$ nanowires, (b and c) SEM images, (d and e) TEM images, (f) HRTEM image, (g) the corresponding SAED pattern and (h) EDS spectrum of the urchin-like $NiCo_2(CO_3)_{1.5}(OH)_3$@$NiCo_2S_4$.

not well-defined micro-/nano-structure, it is a high efficient path to obtain the advanced nanostructure and increase the electrode-electrolyte interface area.[38] Fig. 3c shows the high magnification SEM image of urchin-like $NiCo_2(CO_3)_{1.5}(OH)_3$ @$NiCo_2S_4$. Fig. S3 exhibits the process of morphology transformation from nanowires to urchin-like structure. Fig. S3a shows the nanowires structure with reaction time of 12 h. While the reaction time increases to 16 and 20 h (Fig. S3b and c), the nanowires gradually began aggregating and several nanowires aggregated into the sparse urchin-like structure on the Ni foam. But the reaction time is 24h, a large number of nanowires aggregated into urchin-like structure with nano-branches on the Ni foam. Fig. 3d shows the TEM images of $NiCo_2(CO_3)_{1.5}(OH)_3$@$NiCo_2S_4$ composites, which were obtained by the treatment of ultrasound for 20 min. The enlarged image (Fig. 3e) demonstrates the clear core-shell structure which are the Ni-$Co_2(CO_3)_{1.5}(OH)_3$ is core material and the $NiCo_2S_4$ is shell material with red line separation two parts. Fig. 3f is image of high resolution transmission electron microscope (HRTEM) at the border between core and shell materials. It reveals two interplanar spacings of 0.54 and 0.228 nm, corresponding to

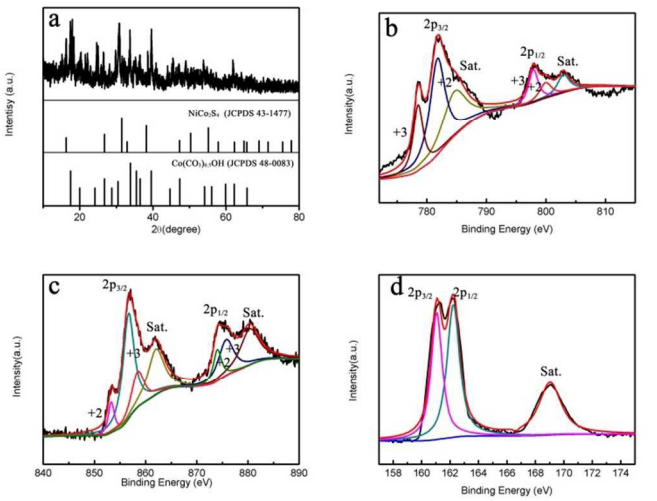

Fig. 4 (a) XRD patterns of $NiCo_2(CO_3)_{1.5}(OH)_3$@$NiCo_2S_4$, XPS spectra of (b) Co 2p, (c) Ni 2p (d) S 2p for the $NiCo_2(CO_3)_{1.5}(OH)_3$@$NiCo_2S_4$.

(111) and (231) lattice planes of the $NiCo_2S_4$ and Ni-$Co_2(CO_3)_{1.5}(OH)_3$, respectively. The diffraction rings of select area electron diffraction (SAED) pattern can be readily indexed to the (440), (422) and (023) planes of the $NiCo_2S_4$ and $NiCo_2(CO_3)_{1.5}(OH)_3$ phases in Fig. 3g, which is consistent with the above analysis. The EDS analysis in Fig. 3h demonstrates that the composite consists of Co, Ni, O, S and C elements, indicating that $NiCo_2(CO_3)_{1.5}(OH)_3$ and urchin-like $NiCo_2(CO_3)_{1.5}(OH)_3$@$NiCo_2S_4$.

Fig. S4 a shows the X-ray diffraction patterns of the urchin-like precursors, $NiCo_2S_4$ and $NiCo_2(CO_3)_{1.5}(OH)_3$ @$NiCo_2S_4$ core-shell powders. The diffraction peaks of blue curve ($NiCo_2(CO_3)_{1.5}(OH)_3$) can be well indexed with $Co(CO_3)_{0.5}OH$ (JCPDS Card no. 48-0083), as shown in Fig.S4 b. Because the Ni ion replacing the partial of Co ions does not change the crystal structure and only slightly changes the lattice parameters.[32] The diffraction peaks of black curve can be well indexed with cubic type $NiCo_2S_4$ (JCPDS Card no. 43-1477). After the NaHS aqueous solution soaking, the sample powders of core-shell structure exhibited the diffraction peaks of precursors and cubic type $NiCo_2S_4$. At the same time, It also demonstrates that the $NiCo_2(CO_3)_{1.5}(OH)_3$@$NiCo_2S_4$ has been successfully synthesized by the ion exchange route from Fig. 4a. The nanomaterial of $NiCo_2(CO_3)_{1.5}(OH)_3$@$NiCo_2S_4$ was further investigated by X-ray photoelectron spectroscopy (XPS) measurements. Fig. 4b-4d shows the typical Co 2p, Ni 2p, S 2p XPS spectrum of $NiCo_2(CO_3)_{1.5}(OH)_3$@$NiCo_2S_4$ core-shell powders sample. The Co 2p, Ni 2p spectrum can be fitted with spin-orbit doublet and shake-up satellites (identified as "Sat."), by using a Gaussian fitting method. As shown in Fig. 4b, the Co 2p spectrum can be best fitted with two spin-orbit doublets, characteristic of Co^{2+} and Co^{3+}, and two shake-up satellites. The Ni 2p spectrum (Fig. 4c) can also be best fitted by considering two spin-orbit doublets characteristic of Ni^{2+} and Ni^{3+} and two shake-up satellites.[32,36] The binding energies at 163.1 and 161.8 eV correspond to S $2p_{1/2}$ and S $2p_{3/2}$, respectively. The component at 163.8 eV is typical of metal–sulphur bonds and the component at 162.6 eV indicates the sulphur ion in low coordination at the surface.[39] According to the XPS spectrum analysis, the near-surface of the sample has a composition has a composition of Co^{2+}, Co^{3+}, Ni^{2+}, Ni^{3+} and S^{2-},which is in good agreement with the Ni-$Co_2(CO_3)_{1.5}(OH)_3$@$NiCo_2S_4$.

3.3 Electrochemical measurement:

The electrochemical performance of the electrode materials is measured in 2M KOH aqueous solution with the three-electrode system. Fig. 5a exhibits the CV curves of the black Ni foam, urchin-like $NiCo_2S_4$, urchin-like precursors, urchin-like $NiCo_2(CO_3)_{1.5}(OH)_3$@$NiCo_2S_4$ and $NiCo_2(CO_3)_{1.5}(OH)_3$ @$NiCo_2S_4$ nanowires at the scan rate of 10 $mV.s^{-1}$. It should be seen that the current density generated by the nickel foam is very low based on the CV areas, as compared with that of the active material. Therefore, the capacitance is mainly attributed to the active materials. All of the curves show the pseudo-capacitive properties, which is attributed to the Faradaic redox reaction. The CV curve of the pure urchin-like $NiCo_2S_4$ electrode demonstrates a visible pair of redox peaks based on the following reaction equation[40]:

$$NiCo_2S_4 + 4OH^- \leftrightarrow NiS_{4-2x}OH + 2CoS_xO + 2H_2O + 4e^-$$

The urchin-like precursors exhibit a pair of redox peaks, because the electrode materials react with the alkaline electro lyte.[41] The emergence of only one pair of redox peaks for the urchin-like $NiCo_2(CO_3)_{1.5}(OH)_3$@$NiCo_2S_4$ electrode should result from the superposition of the peaks of the urchin-like $NiCo_2S_4$ and precursors electrode in alkaline electrolyte.[25,41] Obviously, the peaks current of the urchin-like Ni-$Co_2(CO_3)_{1.5}(OH)_3$@$NiCo_2S_4$ are much higher than the other electrode materials, indicating that the $NiCo_2S_4$ coating on the precursor surface improves the ion diffusion rate and

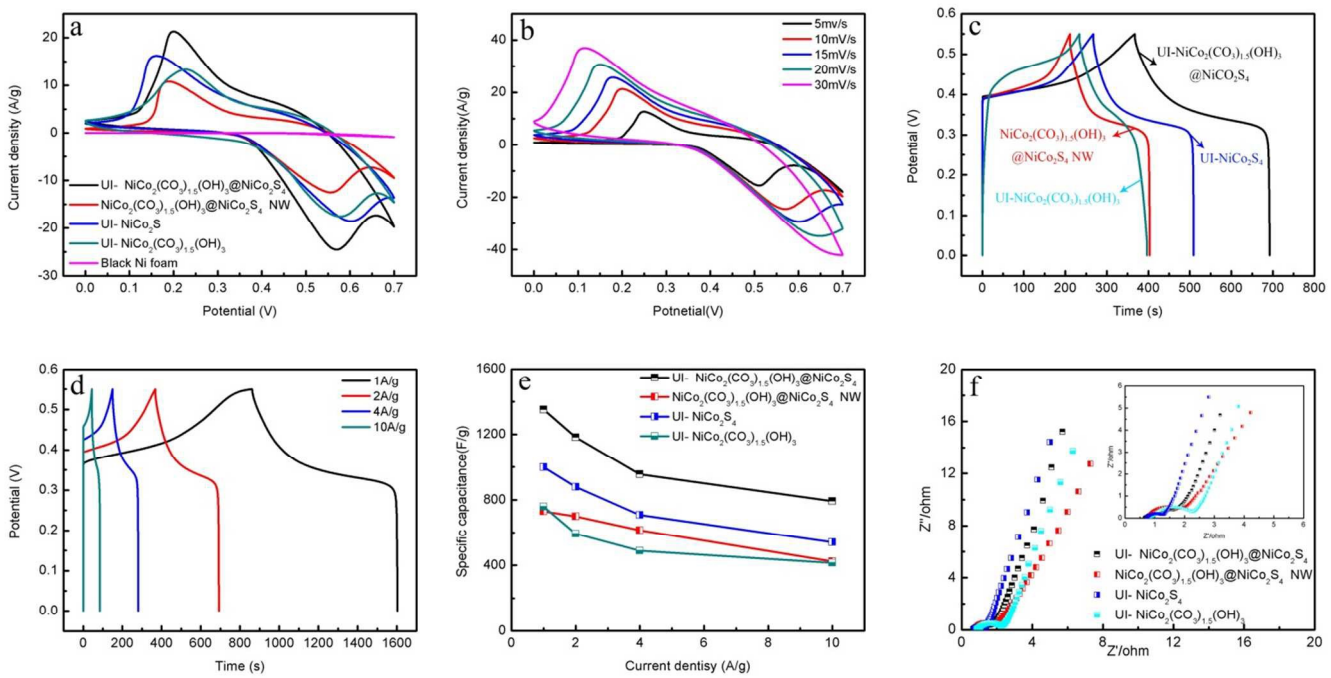

Fig. 5 (a) CV curves of urchin-like $NiCo_2(CO_3)1.5(OH)_3@NiCo_2S_4$ electrode at different scan rate, (b) the CV curves of different electrode at the scan rate of 10 $mV.s^{-1}$, (c) the GCD curves of urchin-like $NiCo_2(CO_3)1.5(OH)_3@NiCo_2S_4$ electrode at different current densities. (d) the GCD curves of different electrode at the current density of 2 $A.g^{-1}$. (e) the area specific capacitance of different electrode as a function of current density plot, (f) EIS of different electrodes,

electrochemical reaction response capacity for the electrode materials.[42]

Fig. 5b shows the cyclic voltammetry (CV) curves of the urchin-like $NiCo_2(CO_3)_{1.5}(OH)_3@NiCo_2S_4$ at different scan rate in the potential range of 0-0.7V. With the scan rate increasing, the anodic and cathodic peak shifted towards positive and negative potential, respectively. This is attribute to the polarization phenomenon which is electron transfer rate is much faster than redox reaction rate on the surface of electrode material.[43]

Fig. 5c shows the GCD curves were further performed on the above-mentioned electrode at the current density of 2 A g^{-1} within a potential window of 0-0.55 V. As expected, the discharge time of urchin-like $NiCo_2(CO_3)_{1.5}(OH)_3@NiCo_2S_4$ electrode demonstrates longer than the other electrodes. It adequately reflects that the core-shell structure exhibits higher specific capacitance than single-phase electrode. At the same time, the connection between core and shell materials was hybrid each other, it maybe aggravate degree of crystal defect and accelerated electron transfer rate on the interface.

Fig. 5d demonstrates the galvanostatic charge-discharge (GCD) curves of the urchin-like $NiCo_2(CO_3)_{1.5}(OH)_3$ $@NiCo_2S_4$ electrode at different current densities. According to the equation (2), the specific capacitance of urchin-like $NiCo_2(CO_3)_{1.5}(OH)_3@NiCo_2S_4$ electrode is 1351, 1181.8, 956.4, 791.6 F g^{-1} at current densities of 1, 2, 4, 10 A g^{-1}. With increasing the current densities, the electron transfer rate is much faster than electrochemical reaction and electrode material has not enough time to taking part in redox reaction, resulting in capacitance decreasing.[44] Fig. S5 exhibits that the GCD curves of the urchin-like $NiCo_2(CO_3)_{1.5}(OH)_3$, $NiCo_2S_4$ and $NiCo_2(CO_3)_{1.5}(OH)_3@NiCo_2S_4$ nanowires at different current densities.

Fig. 6a reveals the specific capacitance of electrode materials at current densities of 1, 2, 4, 10 A g^{-1}. The specific capacitance of urchin-like $NiCo_2(CO_3)_{1.5}(OH)_3@NiCo_2S_4$ electrode is higher than the other electrode materials at the same current densities. According to the energy strorage mechanism for the supercapacitor, the core-shell nanostructure electrode demonstrates can make full use of both components and exhibits a potential synergistic effect which are high electrochemical response capacity and excellent cycle stability, which compared with precursors and urchin-like $NiCo_2S_4$ electrode.[3,45] It

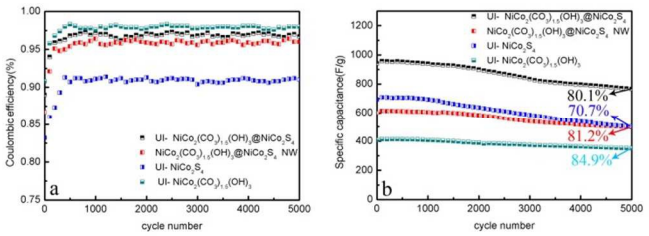

Fig.6 (a) the coulombic efficiency of different electrodes as a function of current density plot, (b) cycling performance of different electrodes at current of 4 A g^{-1}.

means that selecting suitable electrode materials is a key factor to design core-shell nanostructure electrode.

The plots of EIS measurement are shown in Fig. 6b to investigate the rate of charge transfer inside the electrode materials and interface ion absorption-desorption at the open circuit potential in a frequency range from 0.01 to 10^6 Hz. A similar semicircle represents the charge transfer resistance (R_{ct}) in the high frequency region and a linear part represents the Warburg impedance in the low frequency region consist of the Nyquist plots of each electrode. Fig. 6b inset shows the urchin-like $NiCo_2S_4$ have a smaller R_{ct} than the other electrodes, due to Ni and Co element exhibited multi-valence to aggravate degree of crystal defect and accelerated electron transfer rate. As for the urchin-like $NiCo_2(CO_3)_{1.5}(OH)_3$@$NiCo_2S_4$ electrode, it exhibits a smaller R_{ct} than precursors. Meanwhile, it remains a higher slope of line than urchin-like precursors electrode, which indicates that the $NiCo_2(CO_3)_{1.5}(OH)_3$@$NiCo_2S_4$ electrode has urchin-like $NiCo_2(CO_3)_{1.5}(OH)_3$@$NiCo_2S_4$ electrode, it exhibits a smaller R_{ct} than precursors. Meanwhile, it remains a higher slope of line than urchin-like precursors electrode, which indicates that the $NiCo_2(CO_3)_{1.5}(OH)_3$@$NiCo_2S_4$ electrode has a fast charge transfer and interface ion absorption-desorption rate.

Cycle stability is a key factor to evaluate electrochemical performance for the electrode materials which is measured by GCD at the current density of 4 A g^{-1} for 5000 cycles. According to the charge, discharge time and current density in the GCD measurement, it can be calculated the coulombic efficiency by the equation (3):

$$\eta = \frac{t_c}{t_d} \times 100\% \quad (3)$$

Which t_c and td represent the charge, discharge time, η is coulombic efficiency. The coulombic efficiency reflects the degree of electrochemical revisable reaction, indicating that it determined the electrochemical cycle stability. As shown in Fig. 6c, it reveals the relationship between coulombic efficiency and cycle number for four different electrode materials. The precursor electrode has an excellent coulombic efficiency as high as 98% after 5000 cycles, indicating the superior reversible redox reaction and cycle stability. However, the coulombic efficiency of the urchin-like $NiCo_2S_4$ is obviously lower than urchin-like $NiCo_2(CO_3)_{1.5}(OH)_3$. As for the urchin-like $NiCo_2(CO_3)_{1.5}(OH)_3$@$NiCo_2S_4$, the coulombic efficiency is higher than $NiCo_2S_4$ electrode, indicating the precursors improving the core-shell electrode cycle stability and exhibiting a potential synergistic effect.

Fig. 6d shows the specific capacitance of the electrode materials from 1 to 5000 cycle charge-discharge. The $NiCo_2(CO_3)_{1.5}(OH)_3$@$NiCo_2S_4$ NW exhibits higher percentage of the remaining initial capacitance than urchin-like electrode after 5000 cycles. The reason is that the urchin-like $NiCo_2(CO_3)_{1.5}(OH)_3$@$NiCo_2S_4$ has longer electron transfer path than nanowires electrode, lead to increasing percentage of energy loss in the long-time cycle charge-discharge process for the urchin-like electrode materials.

In order to further analyze the cycling performance, the comparison of CV curves before and after cycling at the scan rate of 5 mV s^{-1} has shown in Fig. S6 a. The two curves both appear redox peaks at the same potential, illustrating that the redox reaction doesn't change during cycling. But the peak intensity is weakened, which is caused by the consumption of the active sites. The EIS plots of before and after cycling has shown in Fig. S6 b. A similar semicircle represents the charge transfer resistance (R_{ct}) in the high frequency region and a linear part represents the Warburg impedance in the low frequency region consisting of the Nyquist plots of each electrode. Compared with the before cycling, the EIS plots of after cycling exhibits a larger electrode series resistance (R_s) which can be estimated from the intercept on the real axis and the charge transfer resistance (R_{ct}) at high frequency region. At the low frequency region, the slope of line for the after cycling electrode is larger than the before cycling, indicating that the before cycling electrode exhibits lower diffusion resistance than after cycling and the increase of R_s and R_{ct} affects the pseudocapacitive process. As a result, the cycling performance is attenuated. Fig. S6 c and d show the SEM images of before

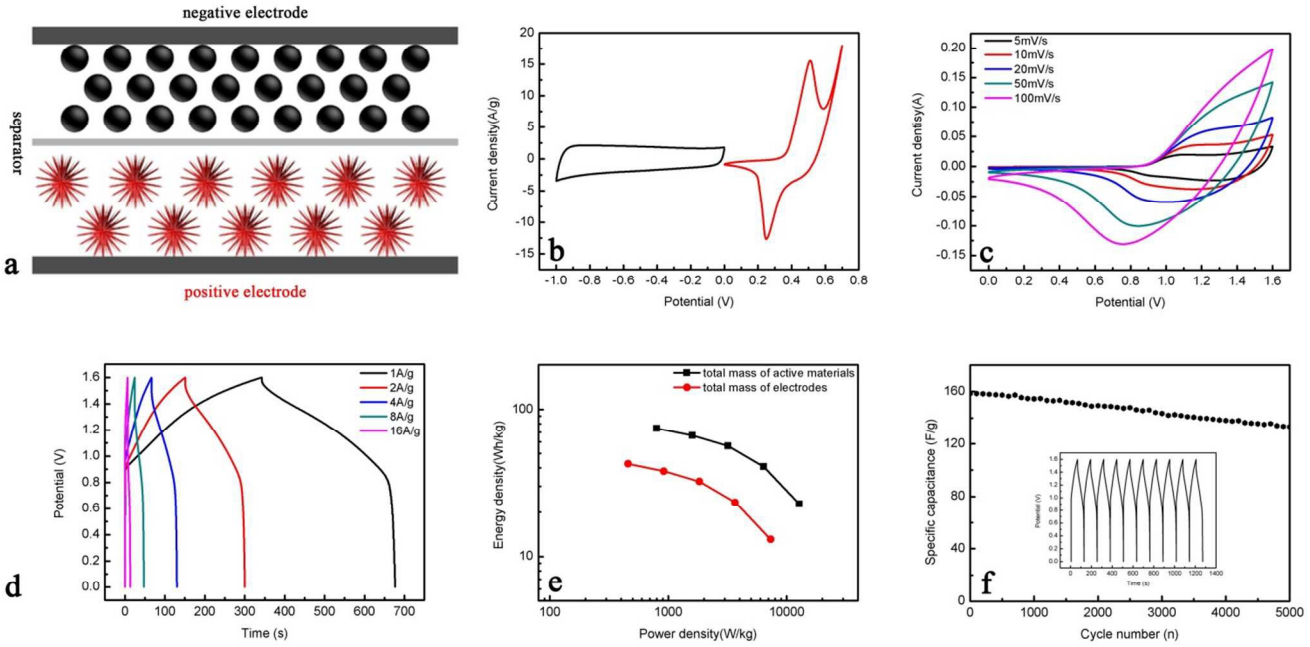

Fig. 7 (a) Schematic illustration of the asymmetric supercapacitor configuration. (b) CV curves of $NiCo_2(CO_3)_{1.5}(OH)_3$@$NiCo_2S_4$ and AC electrodes measured at a scan rate of 10 mV/s in a three-electrode system. (c) CVs and (d) discharge curves of the asymmetric supercapacitor. (e) Ragone plots of the asymmetric supercapacitor. (f) cycling performance of the $NiCo_2(CO_3)_{1.5}(OH)_3$@$NiCo_2S_4$//AC device at current density of 4 A g^{-1} (inset shows the charge-discharge curves of the first 20 cycles.

and after cycling for electrode materials. Both images demonstrated that the micro-architecture doesn't obviously change and the phenomenon demonstrates the electrode material has excellent cycle stability.

According to the high electrochemical response capacity and cycle stability of The urchin-like $NiCo_2(CO_3)_{1.5}(OH)_3$ @$NiCo_2S_4$ electrode in the three-electrode measurement, we conclude that some advantage to apply to the electrode materials. (1) It efficiently motivates synergistic effect for the core-shell structure electrode. The core-shell electrode materials combine the both characteristic: high electrochemical response capacity and excellent cycle stability. (2) The bimetal electrode materials have much electrochemical activity and electron transfer rate than single metal materials, resulting in the core and shell materials exhibits more advantages. Nonetheless, the hybrid crystal intensitied the degree of crystal defect at the interface of core and shell materials. The electron transfer rate is further enhanced. (3) The electroactive materials directly growing on the conductivity substrate, it benefits from improving the materials use ratio in the practical application.

Recently, Ruoff *et al.* recommended the two-electrode electrochemical test is a standard to judge the electrochemical performance of electrode materials. Accordingly, the asymmetric supercapacitor device was successfully assembled, as shown in Fig. 7a. The negative electrode materials were measured by three-electrode system in 2M KOH electrolyte, as shown in Fig. S7. The CV curve shows the double electric layer properties. The specific capacitance is 215.8 F g^{-1} at the current density of 0.5A g^{-1} from the charge-discharge curve. According to the equation of mass distribution ratio calculation, the mass ratio of the positive and negative is 0.29. But the real mass ratio is 0.2, excess negative materials can make full use of positive materials.

Fig. 7b exhibits the CV curves of positive and negative electrodes in three-system electrochemical measurement. The CV curves of asymmetric supercapacitor (Fig.7c) demonstrate a pair of redox peaks at different scan rate from 0-1.6V. It can be clearly seen that the fabricated asymmetric supercapacitor shows a good capacitive behavior with quasi-rectangular CV curves.[13] Fig. 7d shows the GCD measurement at different current densities in potential window of 0-1.6V. It demonstrates a high electrochemical reversibility because the charge curves are symmetry of the corresponding discharge counterparts. The specific capacitance of asymmetric supercapacitor was calculated to be a 208.8, 186.8, 158.5 114.5 64 F.g^{-1} at the

current density of 1, 2, 4, 8, 16 A.g^{-1}, respectively. The energy density and average power density which evaluates standard of asymmetric supercapacitor practical performance was shown in Fig. 7e. Based on the total mass of electroactive materials, the energy densities is 74.2, 66.3, 56.4, 40.7, 22.8 W h kg^{-1} at the average power densities 800, 1600, 3200, 6400, 12800 W kg^{-1}, respectively. The actual energy density and average power density are 42.55 W h kg^{-1} at the average power density of 458.8 W kg^{-1} and 13.05 W h kg^{-1} at the power density of 7340 W kg^{-1}, based on the total mass of electrodes. The actual energy density and average power density are 42.55 W h kg^{-1} at the average power density of 458.8 W kg^{-1} and 13.05 W h kg^{-1} at the power density of 7340 W kg^{-1}. The obtainable real highest energy density (42.55 W. h kg^{-1} at 458.8 W kg^{-1}) based on the mass of electrodes has tremendously surpassed those of most nickel, cobalt or bimetal oxides/sulfides and other typical materials based asymmetric supercapacitors (Table S1, Electronic Supporting Information). Fig. 7f exhibits that the asymmetric supercapacitor has an excellent cycling performance that the overall specific capacitance can still be retained about 81.4% after 5000 cycles.

4. Conclusions

According to the process of architecture design which we presented for the electrode materials, the urchin-like $NiCo_2(CO_3)_{1.5}(OH)_3$@$NiCo_2S_4$ were synthesized by an interface ion exchange. The fabrication process is that the precursors which were obtained by hydrothermal process soaked into the 5mmol L^{-1} NaHS aqueous solution. After the three-system electrochemical measurement, the results gives express to a high electrochemical response capability and long-time cycle stability, where specific capacitance is 956.4 F g^{-1} at current density of 4 A g^{-1} and remains 80.1% overall the capacitance after 5000 cycles. Compared with the single-phase electrode, the core-shell structure electrode material shows a potential synergistic effect which is the core structure of $NiCo_2(CO_3)_{1.5}(OH)_3$ exhibits an outstanding cycle stability and the shell structure exhibits a high electrochemical response capability. The urchin-like $NiCo_2(CO_3)_{1.5}(OH)_3$@$NiCo_2S_4$ asymmetric supercapacitor was fabricated in practical application and exhibited high energy density (32.3W h kg^{-1} at 1835 W kg^{-1}) and cycling stability (retaining 84.1% of overall capacitance after 5000 cycles at current density of 4 A g^{-1}).

Acknowledgements

This work was supported by National Natural Science Foundation of China (51402065), Heilongjiang Province Natural Science Funds for Distinguished Young Scholar (JC201404), Special Innovation Talents of Harbin Science and Technology for Distinguished Young Scholar (2014RFYXJ005), Fundamental Research Funds of the Central University (HEUCFZ), Natural Science Foundation of Heilongjiang Province（B201404）, Program of International S&T Cooperation special project (2013DFR50060), Special Innovation Talents of Harbin Science and Technology (2013RFQXJ145), and the fund for Transformation of Scientific and Technological Achievements of Harbin (2013DB4BG011), Natural Science Foundation of Heilongjiang Province (E201329), Innovation Talents of Harbin Science and Technology (2014RFQXJ035).

[a] *Key Laboratory of Superlight Material and Surface Technology, Ministry of Education, Harbin Engineering University, 150001, P. R. China.*

[b] *State Key Laboratory of Theoretical and Computational Chemistry, Institute of Theoretical Chemistry, Jilin University Changchun, 130023, P. R. China*

[c] *Institute of Advanced Marine Materials, Harbin Engineering University, 150001, P. R. China.*

* *Corresponding author: Tel: +86 451 8253 3026; Fax: +86 451 8253 3026. E-mail address: zhqw1888@sohu.com.cn*

Notes and References

1. B. E. Conway, Electrochemical Supercapacitors: Scientific Fundamentals and Technological Applications, Kulwer Academic, 1999.

2. V. Augustyn, P. Simon and B. Dunn, *Energy & Environmental Science*, 2014, 7, 1597-1614.
3. I. E. Rauda, V. Augustyn, B. Dunn and S. H. Tolbert, *Accounts Chem. Res.*, 2013, 46, 1113-1124.
4. X. Rui, H. Tan and Q. Yan, *Nanoscale*, 2014, 6, 9889-9924.
5. M. R. Gao, Y. F. Xu, J. Jiang and S. H. Yu, *Chem. Soc. Rev.*, 2013, 42, 2986-3017.
6. V. Augustyn, J. Come, M. A. Lowe, J. W. Kim, P. L. Taberna, S. H. Tolbert, H. D. Abruna, P. Simon and B. Dunn, *Nat. Mater.*, 2013, 12, 518-522.
7. A. L. Mohana Reddy, S. R. Gowda, M. M. Shaijumon and P. M. Ajayan, *Adv. Mater.*, 2012, 24, 5045-5064.
8. G. H. Yu, X. Xie, L. J. Pan, Z. N. Bao and Y. Cui, *Nano Energy*, 2013, 2, 213-234.
9. X. Wang, X. Lu, B. Liu, D. Chen, Y. Tong and G. Shen, *Adv. Mater.*, 2014, 26, 4763-4782.
10. P. Simon and Y. Gogotsi, *Nat. Mater.*, 2008, 7, 845-854.
11. Q. F. Zhang, E. Uchaker, S. L. Candelaria and G. Z. Cao, *Chem. Soc. Rev.*, 2013, 42, 3127-3171.
12. W. Zhou, X. Cao, Z. Zeng, W. Shi, Y. Zhu, Q. Yan, H. Liu, J. Wang and H. Zhang, *Energy Environ. Sci.*, 2013, 6, 2216.
13. J. Yan, Z. J. Fan, W. Sun, G. Q. Ning, T. Wei, Q. Zhang, R. F. Zhang, L. J. Zhi and F. Wei, *Adv. Funct. Mater.*, 2012, 22, 2632-2641.
14. G. R. Patzke, Y. Zhou, R. Kontic and F. Conrad, *Angew. Chem. Int. Edit.*, 2011, 50, 826-859.
15. J. Jiang, Y. Li, J. Liu, X. Huang, C. Yuan and X. W. Lou, *Adv. Mater.*, 2012, 24, 5166-5180.
16. Z. Qian, T. Peng, J. Wang and L. Qu, *ChemSusChem*, 2014, 1881-1887.
17. L. Bao, J. Zang and X. Li, *Nano Lett.*, 2011, 11, 1215-1220.
18. H. Jiang, P. S. Lee and C. Li, *Energy Environ. Sci.*, 2013, 6, 41-53.
19. X.-C. Dong, H. Xu, X.-W. Wang, Y.-X. Huang, M. B. Chan-Park, H. Zhang, L.-H. Wang, W. Huang and P. Chen, *ACS Nano*, 2012, 6, 3206-3213.
20. R. Liu, J. Duay and S. B. Lee, *Chem. Commun.*, 2011, 47, 1384-1404.
21. D. H. Seo, Z. J. Han, S. Kumar and K. Ostrikov, *Adv. Energy Mater.*, 2013, 3, 1316-1323.
22. M. B. Sassin, C. N. Chervin, D. R. Rolison and J. W. Long, *Accounts Chem. Res.*, 2012, 46, 1062-1074.
23. J.-W. Liu, H.-W. Liang and S.-H. Yu, *Chem. Rev.*, 2012, 112, 4770-4799.
24. Y. Xiong and Y. Xia, *Adv. Mater.*, 2007, 19, 3385-3391.
25. X. Xia, J. Tu, Y. Zhang, X. Wang, C. Gu, X.-b. Zhao and H. J. Fan, *ACS Nano*, 2012, 6, 5531-5538.
26. J. Yan, Q. Wang, T. Wei and Z. Fan, *Adv. Energy Mater.*, 2014, 4, 1-43.
27. D. Yang, *J. Power Sources*, 2012, 198, 416-422.
28. C. Yuan, H. B. Wu, Y. Xie and X. W. Lou, *Angew. Chem. Int. Edit.*, 2014, 53, 1488-1504.
29. L. Hu, L. Wu, M. Liao, X. Hu and X. Fang, *Adv. Funct. Mater.*, 2012, 22, 998-1004.
30. K. B. Xu, W. Y. Li, Q. Liu, B. Li, X. J. Liu, L. An, Z. G. Chen, R. J. Zou and J. Q. Hu, *J. Mater. Chem. A*, 2014, 2, 4795.
31. W. Zhou, D. Kong, X. Jia, C. Ding, C. Cheng and G. Wen, *J. Mater. Chem. A*, 2014, 2, 6310.
32. H. Chen, J. Jiang, L. Zhang, H. Wan, T. Qi and D. Xia, *Nanoscale*, 2013, 5, 8879-8883.
33. S. Peng, L. Li, C. Li, H. Tan, R. Cai, H. Yu, S. Mhaisalkar, M. Srinivasan, S. Ramakrishna and Q. Yan, *Chem Commun.*, 2013, 49, 10178-10180.
34. X. Xia, C. Zhu, J. Luo, Z. Zeng, C. Guan, C. F. Ng, H. Zhang and H. J. Fan, *Small*, 2014, 10, 766-773.
35. Z. Xing, Q. Chu, X. Ren, C. Ge, A. H. Qusti, A. M. Asiri, A. O. Al-Youbi and X. Sun, *J. Power Sources*, 2014, 245, 463-467.
36. Q. Liu, J. Jin and J. Zhang, *ACS Appl. Mater. Inter.*, 2013, 5, 5002-5008.
37. W. Zhao, X. Zhu, H. Bi, H. Cui, S. Sun and F. Huang, *J. Power Sources*, 2013, 242, 28-32.
38. J. Liu, J. Jiang, C. Cheng, H. Li, J. Zhang, H. Gong and H. J. Fan, *Adv. Mater.*, 2011, 23, 2076-2081.
39. J. Pu, F. Cui, S. Chu, T. Wang, E. Sheng and Z. Wang, *ACS Sustain. Chem. Eng.*, 2014, 2, 809-815.
40. H. Chen, J. Jiang, L. Zhang, D. Xia, Y. Zhao, D. Guo, T. Qi and H. Wan, *J. Power Sources*, 2014, 254, 249-257.
41. J. Xiao, L. Wan, S. Yang, F. Xiao and S. Wang, *Nano Lett.*, 2014, 14, 831-838.
42. L. Yu, N. Shi, Q. Liu, J. Wang, B. Yang, B. Wang, H. Yan, Y. Sun and X. Jing, *Phys. Chem. Chem. Phys.*, 2014, 16,

17936-17942.

43. B. Wang, Q. Liu, Z. Qian, X. Zhang, J. Wang, Z. Li, H. Yan, Z. Gao, F. Zhao and L. Liu, *J. Power Sources*, 2014, 246, 747-753.
44. L. Mei, T. Yang, C. Xu, M. Zhang, L. Chen, Q. Li and T. Wang, *Nano Energy*, 2014, 3, 36-45.
45. F. Y. Ning, M. F. Shao, C. L. Zhang, S. M. Xu, M. Wei and X. Duan, Nano Energy, 2014, 7, 134-142.

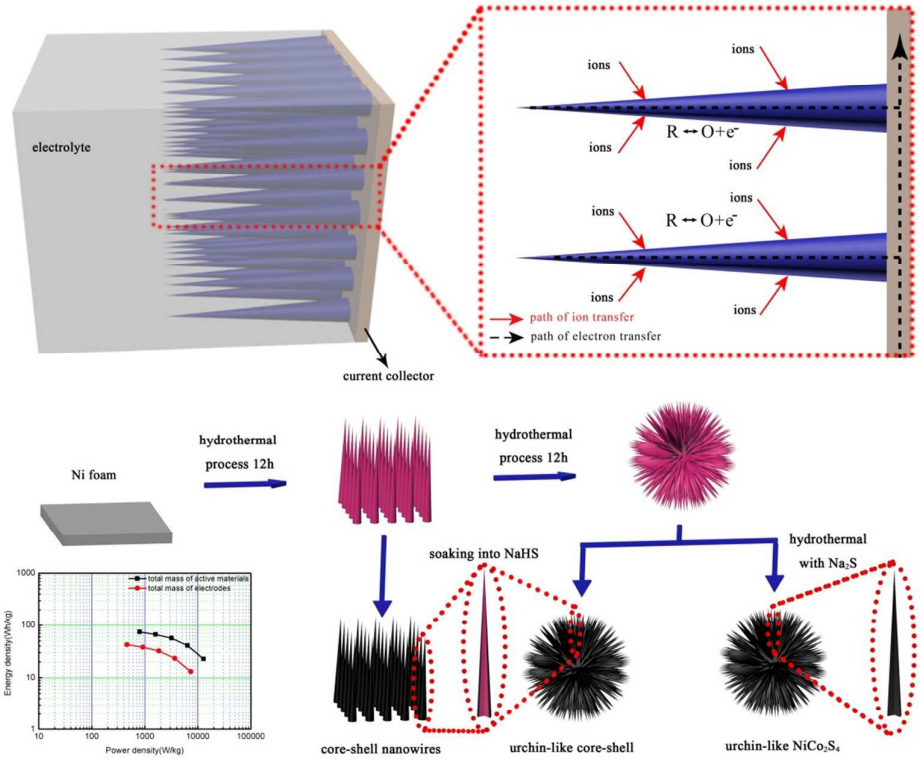

Based on the electron and ion transfer process from the electrochemistry behavior, the urchin-like $NiCo_2(CO_3)_{1.5}(OH)_3$@$NiCo_2S_4$ has been successfully synthesized by the hydrothermal process and ion exchange route. Meanwhile, the core-shell nanostructure electrode demonstrates can make full use of both components and exhibits a potential synergistic effect which are high electrochemical response capacity and excellent cycle stability, which compared with precursors and urchin-like $NiCo_2S_4$ electrode. The Ni foam as the conductivity substrates can provide more sites to load more electroactive materials (electroactive mass of urchin-like core-shell structure: 6.4 mg. cm^{-3}), resulting in a high actual energy and power densities for the aqueous asymmetric supercapacitor.